Computer and Telecommunication Engineering 2024, 2(4), 2846.
https://doi.org/10.54517/cte2846

Article

Outage performance of users in CR-NOMA network systems

Huu Q. Tran

Faculty of Electronics Technology (FET), Industrial University of Ho Chi Minh City (IUH), Ho Chi Minh City 700000, Vietnam;
tranquyhuu@iuh.edu.vn

CITATION

Tran HQ. Outage performance of users in CR-NOMA network systems. Computer and Telecommunication Engineering. 2024; 2(4): 2846. https://doi.org/10.54517/cte2846

ARTICLE INFO

Received: 23 August 2024
Accepted: 9 October 2024
Available online: 26 October 2024

COPYRIGHT

Copyright © 2024 by author(s). *Computer and Telecommunication Engineering* is published by Asia Pacific Academy of Science Pte. Ltd. This work is licensed under the Creative Commons Attribution (CC BY) license. https://creativecommons.org/licenses/by/4.0/

Abstract: Non-Orthogonal Multiple Access (NOMA) and Cognitive Radio (CR) technologies present viable solutions to mitigate spectrum scarcity in wireless communication systems. This paper focuses on evaluating the performance of CR-NOMA networks, particularly for user devices operating under a Simultaneous Wireless Information and Power Transfer (SWIPT) framework. We derive explicit mathematical expressions for key performance metrics, including outage probability (OP) and system throughput, as they relate to various power allocation coefficients. Comprehensive simulations are conducted to validate our theoretical findings, revealing that appropriate power allocation significantly impacts user fairness and overall network throughput. The analysis covers a wide range of realistic channel conditions, including Rayleigh fading, to ensure robustness. Additionally, our study addresses the challenge of limiting interference to the primary network by optimizing the transmission power of secondary users while adhering to interference constraints. The results show that the primary user device (D_1) consistently outperforms the secondary user device (D_2), emphasizing the importance of strategic resource management. These contributions provide deeper insights into the factors affecting outage performance in CR-NOMA systems, offering effective solutions for enhancing the robustness, fairness, and efficiency of next-generation wireless communication networks.

Keywords: cognitive radio; cooperative relaying; non-orthogonal multiple access; simultaneous wireless information and power transfer

1. Introduction

Recently, cognitive radio networks (CRNs) have emerged as a promising approach to tackle spectrum scarcity and enhance wireless communication efficiency. CRNs facilitate dynamic spectrum access, enabling secondary users to opportunistically use underutilized spectrum bands without interfering with primary users [1]. This functionality not only reduces spectrum congestion but also improves overall network utilization and flexibility [2]. The advent of dynamic spectrum access has spurred substantial progress in wireless communication, leading to innovative network architectures and protocols [3]. An example of progress in this area is the incorporation of non-orthogonal multiple access (NOMA) into CRNs. NOMA is a multiple access technique that allows multiple users to share the same frequency band simultaneously by using different power levels. This enables higher spectral efficiency and increased connectivity compared to traditional orthogonal multiple access (OMA) schemes.

NOMA is an advanced multiple access technique that enables numerous users to utilize the same frequency resources by distinguishing their signals based on power levels. This method can greatly improve spectral efficiency and user connectivity, especially in environments with a high density of users or fluctuating channel

conditions [4]. Unlike traditional OMA schemes, NOMA allocates different power levels to users based on their channel conditions, allowing simultaneous transmission and reception over the same frequency band. This results in higher spectral efficiency and better resource utilization. In addition, NOMA's ability to handle a larger number of connections makes it particularly suitable for next-generation networks, including LTE and 5G, where the demand for high data rates and low latency is critical. By leveraging the power domain for multiple access, NOMA also enhances user fairness and system throughput, making it a promising solution for the challenges posed by future wireless communication systems [5–9].

The integration of CRNs with NOMA, referred to as cooperative relaying NOMA (CR-NOMA), presents a compelling method for boosting network performance. This combination harnesses the benefits of both technologies: CRNs offer adaptable spectrum access and effective use of available frequency bands, while NOMA allows multiple users to simultaneously use the same frequency resources through power-domain multiplexing. This collaboration enhances spectral efficiency, user connectivity, and network capacity, especially in environments with dense user populations or fluctuating channel conditions [10]. CR-NOMA leverages the inherent advantages of CRNs, such as dynamic spectrum management and interference mitigation, to enhance overall spectrum utilization efficiency. By integrating NOMA, which differentiates users based on their channel conditions and assigns power levels accordingly, CR-NOMA can support a higher number of simultaneous connections. This is particularly advantageous in scenarios where spectrum resources are scarce or highly variable. The combined approach not only maximizes throughput but also reduces latency and improves the quality of service for end-users [11]. Additionally, the cooperative relaying aspect of CR-NOMA facilitates improved communication reliability and extended coverage. Relays can help forward signals to users with poor channel conditions, thereby enhancing network robustness. This is crucial for achieving seamless connectivity in both urban and rural environments, where users may experience varying signal strengths due to obstacles or distance from the base station. Furthermore, CR-NOMA's capability to manage interference and allocate resources efficiently positions it as a promising solution for future wireless communication systems, including beyond 5G (B5G) networks [12]. The impact of Maximum Ratio Combining (MRC) diversity techniques on the performance of cognitive radio systems is analyzed in this study. The author investigates both the ergodic capacity and the average symbol error rate (SER) of the system, providing new expressions for their asymptotic performance. The findings indicate that MRC can achieve full diversity order, with system capacity increasing logarithmically with the number of receive antennas [13]. In [14], the authors propose an opportunistic selection scheme, ODF–AF, for cognitive relay networks, which allows the relay to switch between decode-and-forward (DF) and amplify-and-forward (AF) modes based on channel conditions. The study also investigates the traditional ODF scheme, where the relay alternates between DF and direct transmission. Approximate outage probability expressions are derived for both schemes, and simulation results demonstrate that ODF–AF and ODF outperform traditional DF and direct transmission, showing improved outage performance under transmit power and interference constraints in cognitive systems. In [15], the author proposes and investigates four

novel amplify-and-forward (AF) relaying schemes for both primary (PU) and cognitive users (CU), allowing them to share the same relay. These schemes, namely parallel-transmission-and-parallel-forwarding (PTPF), parallel-transmission-and-serial-forwarding (PTSF), serial-transmission-and-parallel-forwarding (STPF), and serial-transmission-and-serial-forwarding (STSF), optimize the relay transmission process. The study focuses on minimizing total power consumption while maintaining quality of service (QoS) for both users. A key contribution is the introduction of a new performance metric called relay sharing (RS) probability, with closed-form expressions and approximations derived for various schemes. The results demonstrate that the proposed methods can effectively reduce power consumption while ensuring efficient relay sharing.

Despite these advancements, several challenges remain in optimizing the performance of CR-NOMA systems. One significant issue is the outage probability (OP) experienced by users, which directly impacts the reliability and efficiency of the network. The outage probability is influenced by various factors such as power allocation, user location, channel conditions, and interference levels. Addressing these challenges is crucial for the successful deployment and operation of CR-NOMA networks.

In response to these challenges, our paper delves into the analysis of a cooperative FD-NOMA network supported by simultaneous wireless information and power transfer (SWIPT) operating under the time-switching (TS) protocol. In the course of our research, we conduct a thorough analysis using both system simulations and analytical expressions to evaluate the outage probability for users. The main contributions of our paper can be summarized as follows:

- Evaluating the performance of user devices in cognitive NOMA systems based on SWIPT.
- Presenting explicit mathematical formulas for key performance metrics, such as OP and system throughput, in relation to different power allocation coefficients.
- Conducting comprehensive simulations to validate our theoretical findings.

Our research aims to provide a deeper understanding of the factors affecting outage performance in CR-NOMA systems and propose effective solutions to mitigate these issues, thereby contributing to the advancement of next-generation wireless communication technologies.

The remainder of the paper is organized as follows. Section II provides the system model. Section III explores the performance analysis. Section IV addresses the numerical results and discussion. Finally, Section V concludes the paper.

2. System model

We assume a cognitive radio (CR) system model comprising a primary destination (PD) located within the primary network (PN), a secondary source (B), a relay node (R) operating in half-duplex mode, and two destinations, D_1 and D_2. The model utilizes Rayleigh fading channels u with channel gains denoted as Ω_u. The channels, as indicated in **Figure 1**, include the secondary source to destination (C_{SD}), secondary source to relay (C_{SR}), relay to destination D_1 (C_{RD_1}), and relay to destination D_2 (C_{RD_2}). These channels are modeled as complex Gaussian random variables (RVs)

with zero mean and are independent and identically distributed (i.i.d.). In this model, each node employs a single antenna, and perfect channel state information (CSI) is assumed to be available for all nodes. The relay node (R) is positioned sufficiently far from the primary destination (PD) to avoid interfering with the primary network, as illustrated in **Figure 1**. Both primary and secondary networks operate under specific power constraints to ensure optimal performance without causing undue interference. The key parameters used in the model and throughout the paper are defined in **Table 1**, providing a comprehensive overview of the system specifications. This setup allows us to analyze the OP and system throughput under various conditions, including different power allocation coefficients, channel gain values, and interference levels. By understanding these dynamics, we can optimize the placement of relay stations and adjust system parameters to enhance performance at D_1 and D_2 within the NOMA system.

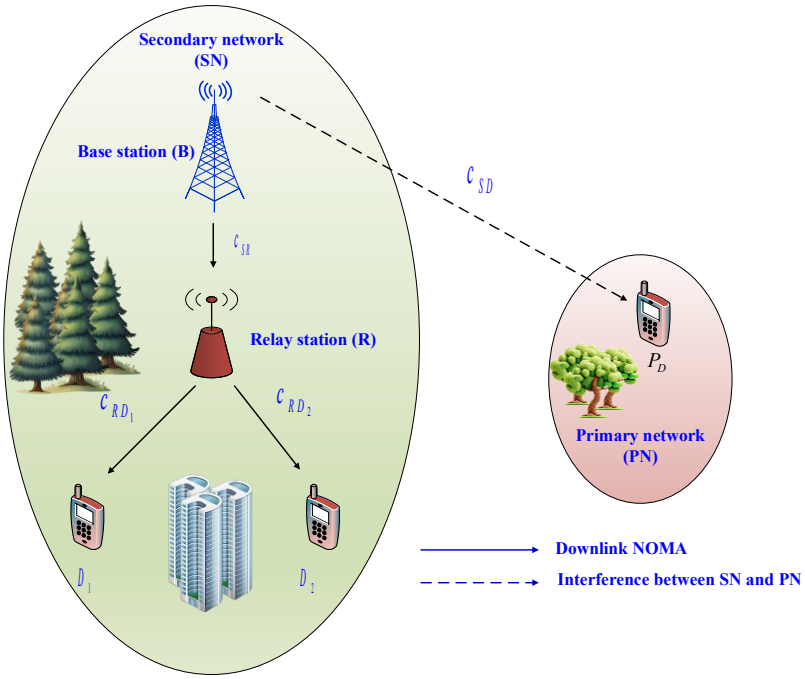

Figure 1. System model.

Table 1. Definition of Symbols.

Symbol	Definition
P_B	Transmit power at B
$\overline{P_B}$	Maximum average transmit power at B
|cSD|2	Power gain of B → PD
|cSR|2	Power gain of B → R
|cRD1|2	Power gain of R → D1
|cRD2|2	Power gain of R → D2
I	Maximum allowable noise at the destination in the primary network P_D.
$w_R(k)$	Nhiễu Gauss trắng cộng (AWGN) tại R với phương sai bằng σ_R^2.
$\rho_R = \frac{P_R}{\sigma_{RD_i}^2}$	Tỷ số tín hiệu trên nhiễu tại Di, $i \in \{1,2\}$.

Table 2. Comparison of our work with those in references [13], [14], and [15].

Criteria	Work in [13]	Work in [14]	Work in [15]	My work
Main Topic	Impact of Maximum Ratio Combining (MRC) on the performance of cognitive radio systems.	Proposal of ODF–AF selection mechanism for cognitive relay networks, compared with traditional transmission modes.	New amplification and forwarding relay mechanisms for primary and secondary users in shared relay networks.	Outage performance in CR-NOMA networks, studying power allocation effects and secondary user performance.
Techniques or Research Models	MRC technique, average rate and symbol error rate (SER) analysis, diversity calculations.	ODF–AF mechanism, error probability decomposition, comparisons of DF and AF modes.	New relay mechanisms like PTPF, PTSF, STPF, STSF, optimizing power consumption and ensuring quality of service (QoS).	Performance analysis in CR-NOMA with SIC, deriving outage probabilities and system performance based on power allocation and channel conditions.
Key Results	MRC achieves full diversity, system performance increases logarithmically with the number of receiving antennas.	ODF–AF and ODF outperform traditional DF and direct transmission, with approximate error probability expressions.	New relay mechanisms reduce power consumption and improve performance through optimizing relay sharing probabilities.	Clear formulas for outage probabilities of secondary users in CR-NOMA, improving performance through power allocation and analysis of practical channel conditions.
Research Methodology	Theoretical calculations for MRC performance, exact asymptotic performance expressions.	Theoretical and simulation comparisons for different relay mechanisms, error probability analysis.	Proposing and analyzing new relay mechanisms, calculating and comparing new performance metrics like relay sharing probabilities.	Theoretical and simulation analysis of user performance in CR-NOMA, calculating outage probabilities and system performance under different conditions.
Specific Application	Cognitive radio systems using MRC to enhance performance.	Cognitive relay networks with ODF–AF mechanism, compared to traditional modes.	Amplification and forwarding relay mechanisms for primary and secondary users in shared relay networks.	CR-NOMA networks with power allocation strategies and performance analysis under various channel conditions.
Simulation Results	Not specifically mentioned in the description.	Includes simulation results for ODF–AF and traditional mechanisms, performance comparisons.	Analysis expressions and simulation results for new relay mechanisms, comparing performance and power consumption.	Simulation and theoretical results for outage performance and system under various conditions, particularly focusing on power allocation and channel conditions.
Practical Implications	Enhances understanding of MRC performance in cognitive radio systems.	Provides a new relay selection method, improving performance in cognitive networks.	Optimizes power and QoS in shared relay networks, applicable to relay and communication networks.	Provides formulas and simulations for secondary user performance in CR-NOMA, aiding future network deployment and improving spectrum utilization.

$$\gamma_{RD_2,x_1} = \frac{\rho_R \alpha_1 \left|c_{SRD_2}\right|^2}{\rho_R \alpha_2 \left|c_{SRD_2}\right|^2 + 1} \tag{7}$$

Then, by reducing the existing noise as described in Equation (7), the remaining signal can be detected more effectively. This noise reduction enhances the signal clarity, enabling more accurate detection of the transmitted signal. Specifically, to detect its own signal (x_2) at destination D_2, the SNR must be calculated. The SNR at D_2 is determined based on the following formula:

$$\gamma_{RD_2,x_2} = \rho_R \alpha_2 \left|c_{RD_2}\right|^2 \text{ (8)} \tag{8}$$

Note that D_1 is allocated a higher power allocation coefficient than D_2 ($\alpha_1 > \alpha_2$), meaning that the signal x_1 has a higher detection priority compared to x_2. This

prioritization affects the detection process and the calculation of the SINR. In this case, the SINR at D_1, considering the interference from x_2, can be expressed as:

$$\gamma_{RD_1,x_1} = \frac{\rho_R \alpha_1 \left|c_{RD_1}\right|^2}{\rho_R \alpha_2 \left|c_{RD_1}\right|^2 + 1} \tag{9}$$

3. Performance analysis

For a Rayleigh fading channel with an exponential distribution, the OP is calculated based on the probability density function (PDF) and cumulative distribution function (CDF) of the channel gain c_i, as given in [18]. The OP is a critical measure of the system's reliability, indicating the probability that the received signal falls below a certain threshold, leading to an outage.

The PDF of the channel gain c_i in a Rayleigh fading channel is given by:

$$f_{|c_i|^2}(x) = \frac{1}{\Omega_{c_i}} \times e^{-x\frac{1}{\Omega_{c_i}}} \tag{10}$$

where Ω_{c_i} is the average power of the channel gain.

The CDF of the channel gain is:

$$F_{|c_i|^2}(x) = 1 - e^{-x\frac{1}{\Omega_{c_i}}} \tag{11}$$

The received instantaneous SNR(γ) is considered a random variable (RV). If γ is lower than a permissible threshold, the receiver may fail to successfully recover the transmitted signal. In this case, the OP is used to evaluate the system's performance during fading when the channel's time coherence is considerably large compared to the symbol period. OP is the probability that the received SNR(γ) is less than the threshold SNR(γ_{thr}) [16–18]. Mathematically, the OP is expressed as follows:

$$OP = \int_0^{\gamma_{thr}} f_\gamma(\gamma) d\gamma \; = P_r(\gamma < \gamma_{thr}) = F_\gamma(\gamma_{thr}) \; = P_r(\gamma < \gamma_{thr}) = \int_0^{\gamma_{thr}} f_\gamma(\gamma) d\gamma \tag{13}$$

In [19], the relationship between the CDF and PDF is demonstrated.

3.1. Outage probability at D_1

The OP at D_1 is the probability that the achieved rate is less than the predefined threshold rate. This threshold rate is a critical parameter that determines the minimum acceptable performance level for reliable communication.

$$\mathrm{O}P_{D_1} = P_r(R_1 < R_{thr})$$

Therefore, the OP of x_1 at D_1 can be given by:

$$OP_{D_1} = P_r\left[min\left(\gamma_{R,x_1}, \gamma_{RD_1,x_1}\right) < \gamma_1\right] = 1 - P_r\left(\gamma_{R,x_1} > \gamma_1, \gamma_{RD_1,x_1} > \gamma_1\right)$$
$$= 1 - \begin{bmatrix} P_r\left(\frac{\overline{P_B}\alpha_1|c_{SR}|^2}{\overline{P_B}\alpha_2|c_{SR}|^2 + 1} > \gamma_1, \frac{\rho_R\alpha_1\left|c_{RD_1}\right|^2}{\rho_R\alpha_2\left|c_{RD_1}\right|^2 + 1} > \gamma_1, \overline{P_{BS}} < \frac{\rho_I}{|c_{SD}|^2}\right) + \\ P_r\left(\frac{\overline{P_I}\alpha_1|c_{SR}|^2}{\overline{P_I}\alpha_2|c_{SR}|^2 + |c_{SD}|^2} > \gamma_1, \frac{\rho_R\alpha_1\left|c_{RD_1}\right|^2}{\rho_R\alpha_2\left|c_{RD_1}\right|^2 + 1} > \gamma_1, \overline{P_B} > \frac{\rho_I}{|c_{SD}|^2}\right) \end{bmatrix} \quad (14)$$

We set:

$$A_1 = P_r\left(\frac{\overline{P_B}\alpha_1|c_{SR}|^2}{\overline{P_B}\alpha_2|c_{SR}|^2 + 1} > \gamma_1, \frac{\rho_R\alpha_1\left|c_{RD_1}\right|^2}{\rho_R\alpha_2\left|c_{RD_1}\right|^2 + 1} > \gamma_1, \overline{P_B} < \frac{\rho_I}{|c_{SD}|^2}\right)$$

$$A_2 = P_r\left(\frac{\overline{P_I}\alpha_1|c_{SR}|^2}{\overline{P_I}\alpha_2|c_{SR}|^2 + |c_{SD}|^2} > \gamma_1, \frac{\rho_R\alpha_1\left|c_{RD_1}\right|^2}{\rho_R\alpha_2\left|c_{RD_1}\right|^2 + 1} > \gamma_1, \overline{P_B} > \frac{\rho_I}{|c_{SD}|^2}\right)$$

$$OP_{D_1} = 1 - (A_1 + A_2) \quad (15)$$

where $\varrho_I = \frac{I}{\sigma_{PD}^2}$and $\gamma_1 = 2^{2R1} - 1$ are the SNR related to interference in the primary network and the SNR related to the target rate R_1 of D_1, respectively. Based on the distribution of the wireless channels, it is expressed as:

$$A_1 = P_r(|c_{SR}|^2 > \frac{\psi}{\overline{P_B}}, \left|c_{RD_1}\right|^2 > \frac{\psi}{\rho_R}, |c_{RD}|^2 < \frac{\rho_I}{\overline{P_B}})$$

According to Equation (13), A_1 can be calculated as follows:

$$A_1 = \int_{\frac{\psi}{\overline{P_B}}}^{\infty} f_{|c_{SR}|^2}(x)dx \int_{\frac{\psi}{\rho_R}}^{\infty} f_{\left|c_{RD_1}\right|^2}(y)dy \int_0^{\frac{\rho_I}{\overline{P_B}}} f_{|c_{SD}|^2}(z)dz$$
$$= \int_{\frac{\psi}{\overline{P_B}}}^{\infty} (\frac{1}{\Omega_{c_{SR}}} \times e^{-x\frac{1}{\Omega_{c_{SR}}}})(x)dx \times \int_{\frac{\psi}{\rho_R}}^{\infty} \left(\frac{1}{\Omega_{c_{RD_1}}} \times e^{-x\frac{1}{\Omega_{c_{SD}}}}\right)(y)dy \times \int_{+0}^{\frac{\rho_I}{\overline{P_B}}} \frac{1}{\Omega_{c_{SD}}} \times e^{-x\frac{1}{\Omega_{c_{SD}}}}(z)dz$$
$$= (-e^{-x\frac{1}{\Omega_{c_{SR}}}})\Big|_{\frac{\psi}{\overline{P_B}}}^{\infty} \times (-e^{-x\frac{1}{\Omega_{c_{RD_1}}}})\Big|_{\frac{\psi}{\rho_R}}^{\infty} \times (-e^{-x\frac{1}{\Omega_{c_{SD}}}})\Big|_{0}^{\frac{\rho_I}{\overline{P_B}}} \quad (16)$$
$$= e^{-\frac{\psi}{\overline{P_B}\Omega_{c_{SR}}} - \frac{\psi}{\rho_R\Omega_{c_{RD_1}}}} \times \left(1 - e^{-\frac{\rho_I}{\overline{P_B}\Omega_{c_{SD}}}}\right)$$

where $\psi = \frac{\gamma_1}{(\alpha_1 - \gamma_1\alpha_2)}$ the Equation (10) can be similarly calculated by substituting A_2 using the following formula:

$$A_2 = P_r(|c_{SR}|^2 > \frac{\psi|c_{SD}|^2}{\rho_I}, \left|c_{RD_1}\right|^2 > \frac{\psi}{\rho_R}, |c_{SD}|^2 > \frac{\rho_I}{\overline{P_B}}$$
$$= \int_{\frac{\psi}{\rho_R}}^{\infty} f_{\left|c_{RD_1}\right|^2}(x)dx \int_{\frac{\rho_I}{\overline{P_B}}}^{\infty} \int_{\frac{\psi y}{\rho_I}}^{\infty} f_{|c_{SD}|^2} y dy f_{|c_{SR}|^2}(z)dz$$
$$= \int_{\frac{\psi}{\rho_R}}^{\infty} \frac{1}{\Omega_{c_{RD_1}}} e^{-\frac{x}{\Omega_{c_{RD_1}}}}(x)dx \int_{\frac{\rho_I}{\overline{P_B}}}^{\infty} \frac{1}{\Omega_{c_{SD}}} e^{-y\frac{1}{\Omega_{c_{SD}}} - \frac{\psi y}{\rho_1\Omega_{c_{SR}}}}(y)dy$$

$$= \int_{\frac{\psi}{\rho_R}}^{\infty} \frac{1}{\Omega_{c_{RD_1}}} e^{-\frac{x}{\Omega_{c_{RD_1}}}}(x)dx \int_{\frac{\rho_I}{\overline{P}_{BS}}}^{\infty} \frac{1}{\Omega_{c_{SD}}} e^{-y\left(\frac{1}{\Omega_{c_{SD}}}+\frac{\psi}{\rho_1\Omega_{c_{SR}}}\right)}(y)dy$$

Let A_2=A_{02} x A_{002}

With:

$$A_{02} = \int_{\frac{\psi}{\rho_R}}^{\infty} \frac{1}{\Omega_{c_{RD_1}}} e^{-\frac{x}{\Omega_{c_{RD_1}}}}(x)dx = -e^{-\frac{x}{\Omega_{c_{RD_1}}}}\Big|_{\frac{\psi}{\rho_R}}^{\infty} = -e^{-\frac{\psi}{\rho_R\Omega_{c_{RD_1}}}} \quad \text{and} \quad A_{002} = \frac{1}{\Omega_{c_{SD}}} \times \frac{1}{-\frac{\left(\rho_I\Omega_{c_{SR}}+\psi\Omega_{c_{SD}}\right)}{\Omega_{c_{SD}}\rho_I\Omega_{c_{SR}}}} \times e^{-y\left(\frac{1}{\Omega_{c_{SD}}}+\frac{\psi}{\rho_I\Omega_{c_{SR}}}\right)}\Big|_{\frac{\rho_I}{\overline{P}_B}}^{\infty} =$$

$$-\frac{\rho_I\Omega_{c_{SR}}}{\rho_I\Omega_{c_{SR}}+\psi\Omega_{c_{SD}}} e^{-\frac{\rho_I}{\overline{P}_B}\left(\frac{1}{\Omega_{c_{SD}}}+\frac{\psi}{\rho_I\Omega_{c_{SR}}}\right)}$$

Hence,

$$A_2 = \frac{\rho_I\Omega_{c_{SR}}}{\rho_I\Omega_{c_{SR}}+\psi\Omega_{c_{SD}}} e^{-\frac{\rho_I}{\overline{P}_B}\left(\frac{1}{\Omega_{c_{SD}}}+\frac{\psi}{\rho_I\Omega_{c_{SR}}}\right)-\frac{\psi}{\rho_I\Omega_{c_{RD_1}}}} \tag{17}$$

By substituting (16) and (17) into (15), the close-form OP formula is expressed as:

$$OP_{D_1} = 1 - \left[e^{-\frac{\psi}{\overline{P}_B\Omega_{c_{SR}}}-\frac{\psi}{\rho_R}} \left(1 - e^{-\frac{\rho_I}{\overline{P}_B\Omega_{c_{SD}}}}\right) + \frac{\rho_I\Omega_{c_{SR}}}{\rho_I\Omega_{c_{SR}}+\psi\Omega_{c_{SD}}} e^{-\frac{\rho_I}{\overline{P}_B}\left(\frac{1}{\Omega_{c_{SD}}}+\frac{\psi}{\rho_I\Omega_{c_{SR}}}\right)-\frac{\psi}{\rho_R\Omega_{c_{RD_1}}}} \right] \tag{18}$$

With: $\alpha_1 > \gamma_1\alpha_2$.

3.2. Outage probability at D_2

Assuming that D_1 perfectly removes continuous noise, the probability of detecting the signal x_2 at D_2 can be expressed as follows:

$$OP_{D_2}^{\rho SIC} = P_r(min(\gamma_{R,x_2}, \gamma_{RD_2,x_2}) < \gamma_2 = 1 - Pr(\gamma_{R,x_2} > \gamma_2, \gamma_{RD2,x_2} > \gamma_2)$$

$$= 1 - \left[\begin{matrix} Pr\left(\overline{\rho_B}\alpha_2|c_{SR}|^2 > \gamma_2, \rho_R\alpha_2\left|c_{RD_2}\right|^2 > \gamma_2, \overline{\rho_B} < \frac{\rho_I}{|c_{SD}|^2}\right) \\ + Pr\left(\frac{\rho_I\alpha_2|c_{SR}|^2}{|c_{SD}|^2} > \gamma_2, \rho_R\alpha_2\left|c_{RD_2}\right|^2 > \gamma_2, \overline{\rho_B} > \frac{\rho_I}{|c_{SD}|^2}\right) \end{matrix} \right] \tag{19}$$

Let $B_1 = Pr\left(\overline{\rho_B}\alpha_2|c_{SR}|^2 > \gamma_2, \rho_R\alpha_2\left|c_{RD_2}\right|^2 > \gamma_2, \overline{\rho_B} < \frac{\rho_I}{|c_{SD}|^2}\right)$

$$B_2 = Pr\left(\frac{\rho_I\alpha_2|c_{SR}|^2}{|c_{SD}|^2} > \gamma_2, \rho_R\alpha_2\left|c_{RD_2}\right|^2 > \gamma_2, \overline{\rho_B} > \frac{\rho_I}{|c_{SD}|^2}\right)$$

$$OP_{D_2}^{pSIC} = 1 - (B_1 + B_2) \tag{20}$$

where $\gamma_2 = 2^{2R_2} - 1$, SNR is related to the target rate R_2 of D_2. Here, B_1 and B_2 can be calculated as follows:

$$B_1 = Pr\left(|c_{SR}|^2 > \frac{\psi}{\overline{P_B}\alpha_2}, \left|c_{RD_2}\right|^2 > \frac{\psi}{\rho_R\alpha_2}, |c_{RD}|^2 < \frac{\rho_I}{\overline{P_B}}\right)$$

Based on (13), B_1 can be calculated as:

$$\begin{aligned} B_1 &= \int_{\frac{\gamma_2}{\overline{\rho_B}\alpha_2}}^{\infty} f_{|c_{SR}|^2}(x)dx \int_{\frac{\gamma_2}{\rho_R\alpha_2}}^{\infty} f_{|c_{RD_2}|^2}(y)dy \int_0^{\frac{\rho_I}{\overline{P_B}}} f_{|c_{SD}|^2}(z)dz \\ &= \int_{\frac{\gamma_2}{\overline{\rho_B}\alpha_2}}^{\infty} \left(\frac{1}{\Omega_{c_{SR}}} \times e^{-x\frac{1}{\Omega_{c_{SR}}}}\right)(x)dx \times \int_{\frac{\gamma_2}{\overline{\rho_B}\alpha_2}}^{\infty} \left(\frac{1}{\Omega_{c_{RD_2}}} \times e^{-x\frac{1}{\Omega_{c_{SD_2}}}}\right)(y)dy \times \int_{\frac{\gamma_2}{\overline{\rho_B}\alpha_2}}^{\infty} \left(\frac{1}{\Omega_{c_{SD}}} \times e^{-x\frac{1}{\Omega_{c_{SD}}}}\right)(z)dz \\ &= \left(-e^{-x\frac{1}{\Omega_{c_{SR}}}}\right)\Big|_{\frac{\gamma_2}{\overline{\rho_B}\alpha_2}}^{\infty} \times \left(-e^{-x\frac{1}{\Omega_{c_{RD_2}}}}\right)\Big|_{\frac{\gamma_2}{\overline{\rho_B}\alpha_2}}^{\infty} \times \left(-e^{-x\frac{1}{\Omega_{c_{SD}}}}\right)\Big|_0^{\frac{\rho_I}{\overline{P_B}}} \\ &= e^{-\frac{\gamma_2}{\overline{P_B}\Omega_{c_{SR}}\alpha_2} - \frac{\gamma_2}{\rho_R\Omega_{c_{RD_2}}\alpha_2}} \times \left(1 - e^{-\frac{\rho_I}{\overline{P_B}\Omega_{c_{SD}}}}\right) \quad (21) \end{aligned} \tag{21}$$

Similarly, we have:

$$B_2 = \Pr\left(|c_{SR}|^2 > \frac{\gamma_2|c_{SD}|^2}{\rho_I\alpha_2}, \left|c_{RD_2}\right|^2 > \frac{\gamma_2}{\rho_R\alpha_2}, |c_{SD}|^2 > \frac{\rho_I}{\overline{P}_B}\right)$$

$$= \int_{\frac{\gamma_2}{\rho_R\alpha_2}}^{\infty} f_{|c_{RD_2}|^2}(x)dx \int_{\frac{\rho_I}{\overline{\rho}_B}}^{\infty} \int_{\frac{\gamma_2 y}{\rho_I\alpha_2}}^{\infty} f_{|c_{SD}|^2} y dy f_{|c_{SR}|^2}(z)dydz$$

$$= \int_{\frac{\gamma_2}{\rho_R\alpha_2}}^{\infty} f_{|c_{RD_2}|^2}(x)dx \int_{\frac{\rho_I}{\overline{\rho}_B}}^{\infty} \frac{1}{\Omega_{c_{SD}}} e^{-y\frac{1}{\Omega_{c_{SD}}}} e^{-\frac{\gamma_2 y}{\rho_I\Omega_{c_{SR}}\alpha_2}}(y)dy$$

$$= \int_{\frac{\gamma_2}{\rho_R\alpha_2}}^{\infty} \frac{1}{\Omega_{c_{RD_2}}} e^{-\frac{x}{\Omega_{c_{RD_2}}}}(x)dx \int_{\frac{\rho_I}{\overline{\rho}_B}}^{\infty} \frac{1}{\Omega_{c_{SD}}} e^{-y\left(\frac{1}{\Omega_{c_{SD}}} + \frac{\gamma_2}{\rho_1\Omega_{c_{SR}}\alpha_2}\right)}(y)dy$$

Let $B_2 = B_{02} \times B_{002}$

With: $B_{02} = \int_{\frac{\gamma_2}{\rho_R\alpha_2}}^{\infty} \frac{1}{\Omega_{c_{RD_2}}} e^{-\frac{x}{\Omega_{c_{RD_2}}}}(x)dx = -e^{-\frac{\gamma_2}{\Omega_{c_{RD_2}}}}\Big|_{\frac{\gamma_2}{\rho_R\alpha_2}}^{\infty} = -e^{-\frac{\gamma_2}{\rho_R\Omega_{c_{RD_2}}\alpha_2}} = \int_{\frac{\rho_I}{\overline{\rho}_B}}^{\infty} \frac{1}{\Omega_{c_{SD}}} e^{-y\left(\frac{1}{\Omega_{c_{SD}}} + \frac{\gamma_2}{\rho_I\Omega_{c_{SR}}\alpha_2}\right)}(y)dy$

And

$$B_{002} = \frac{1}{\Omega_{c_{SD}}} \times \frac{1}{-\left(\frac{1}{\frac{1}{\Omega_{c_{SD}}} + \frac{\gamma_2}{\rho_1\Omega_{c_{SR}}\alpha_2}}\right)} \times e^{-y\left(\frac{1}{\Omega_{c_{SD}}} + \frac{\gamma_2}{\rho_1\Omega_{c_{SR}}\alpha_2}\right)}\Big|_{\frac{\rho_I}{\overline{\rho}_B}}^{\infty}$$

$$= -\frac{\rho_I\Omega_{c_{SR}}\alpha_2}{\rho_I\Omega_{c_{SR}}\alpha_2 + \gamma_2\Omega_{c_{SD}}} e^{-\frac{\rho_I}{\overline{\rho}_B}\left(\frac{1}{\Omega_{c_{SD}}} + \frac{\gamma_2}{\rho_1\Omega_{c_{SR}}\alpha_2}\right)}$$

Thus,

$$B_2 = -\frac{\rho_I \Omega_{c_{SR}} \alpha_2}{\rho_I \Omega_{c_{SR}} \alpha_2 + \gamma_2 \Omega_{c_{SD}}} e^{-\frac{\rho_I}{\overline{\rho}_B}\left(\frac{1}{\Omega_{c_{SD}}} + \frac{\gamma_2}{\rho_I \Omega_{c_{SR}} \alpha_2}\right)} - e^{\frac{\gamma_2}{\rho_R \Omega_{c_{RD_2}} \alpha_2}}$$

$$= \frac{\rho_I \Omega_{c_{SR}} \alpha_2}{\rho_I \Omega_{c_{SR}} \alpha_2 + \gamma_2 \Omega_{c_{SD}}} e^{-\frac{\rho_I}{\overline{\rho}_B}\left(\frac{1}{\Omega_{c_{SD}}} + \frac{\gamma_2}{\rho_I \Omega_{c_{SR}} \alpha_2}\right) - \frac{\gamma_2}{\rho_R \Omega_{c_{RD_2}} \alpha_2}}$$

By substituting (21) and (22) into (20), the OP formula under perfect SIC conditions at D_2 is determined as:

$$OP_{D_2}^{\rho SIC} = 1 - \left[e^{-\frac{\gamma_2}{\overline{\rho}_R \Omega_{c_{SR}} \alpha_2} - \frac{\gamma_2}{\rho_R \Omega_{c_{RD_2}} \alpha_2}} \left(1 - e^{\frac{\rho_I}{\overline{\rho}_B \Omega_{c_{SD}}}}\right) + \frac{\rho_I \Omega_{c_{SR}} \alpha_2}{\rho_I \Omega_{c_{SR}} \alpha_2 + \gamma_2 \Omega_{c_{SD}}} e^{-\frac{\rho_I}{\overline{\rho}_B}\left(\frac{1}{\Omega_{c_{SD}}} + \frac{\gamma_2}{\rho_I \Omega_{c_{SR}} \alpha_2}\right) - \frac{\gamma_2}{\rho_R \Omega_{c_{RD_2}} \alpha_2}} \right] \quad (23)$$

3.3. Asymptotic analysis

In this section, we present performance approximation formulas as additional detailed information about the composite system. These formulas provide a comprehensive understanding of the system's behavior under various conditions, enabling more precise performance evaluations.

When $\rho \to \infty$, it can be applied $e^{-x} \approx 1 - x$. The asymptotic OP at D_1 is calculated as follows:

$$OP_{asym,D_1}^{\infty} = 1 - \left[\left(1 - \frac{\psi}{\overline{\rho}_B \Omega_{c_{SR}}} - \frac{\psi}{\rho_R}\right) \times \frac{\rho_I}{\overline{\rho}_B \Omega_{c_{SD}}} + \frac{\rho_I \Omega_{c_{SR}}}{\rho_I \Omega_{c_{SR}} + \psi \Omega_{c_{SD}}} \times \left(1 - \frac{\rho_I}{\overline{\rho}_B \Omega_{c_{SD}}} - \frac{\psi \rho_I}{\rho_I \overline{\rho}_B \Omega_{c_{SR}}} - \frac{\psi}{\rho_R \Omega_{c_{RD_1}}}\right) \right] \quad (24)$$

The approximate OP at D_2 is calculated by the following expression:

$$OP_{asym,D_2}^{\infty,\rho SIC} = 1 - \left[\begin{array}{l} \left(1 - \frac{\gamma_2}{\overline{\rho}_B \Omega_{c_{SR}} \alpha_2} - \frac{\gamma_2}{\rho_R \alpha_2 \Omega_{c_{RD_2}}}\right) \times \frac{\rho_I}{\overline{\rho}_B \Omega_{c_{SD}}} + \frac{\rho_I \Omega_{c_{SR}} \alpha_2}{\rho_I \Omega_{c_{SR}} \alpha_2 + \gamma_2 \Omega_{h_{SD}}} \\ \times \left(1 - \frac{\rho_I}{\overline{\rho}_B \Omega_{h_{SD}}} - \frac{\gamma_2 \rho_I}{\rho_I \overline{\rho}_B \Omega_{h_{SR}} \alpha_2} - \frac{\gamma_2}{\rho_R \alpha_2 \Omega_{c_{RD_2}}}\right) \end{array} \right] \quad (25)$$

3.4. System throughput

System throughput measures the volume of data or the number of transactions a system can process within a specific timeframe. In communication systems, it usually reflects the rate at which data is reliably sent from a source to its destination. To calculate the throughput for each user device, use the following formula:

$$\tau_{D_i} = (1 - OP_{D_i}) R_i \quad (26)$$

where $i \in \{1,2\}$.

4. Numerical results and discussion

In this content, we evaluate the performance of the CR-NOMA system, where the OP at devices D_1 and D_2 is given by explicit expressions and approximate expressions, respectively, in Equations (14), (18), (19), (23), (24), and (26). The

system throughput is determined by Equation (26). The Monte-Carlo simulation results are consistent with the analytical results across the entire SNR range. The simulations are conducted under the following cases:

Case 1: The simulation parameters were set with specific power allocation coefficients $\alpha_1 = 0.8$, $\alpha_2 = 0.2$, target rates $R_1 = 1bps/Hz$, $R_2 = 2bps/Hz$, and channel gain values ($\Omega_{c_{SR}} = 1, \Omega_{c_{SD}} = 1, \Omega_{c_{RD_1}} = 0.8, \Omega_{c_{RD_2}} = 1.1$), interference between the primary network and SNR, $\varrho_I = 40dB$. The power allocation coefficients determine how power is distributed between different users, while the target rates specify the desired transmission rates for D_1 and D_2. The channel gain values reflect the strength of the signals received at D_1 and D_2, as well as the interference from the primary network. The interference between the primary network and the secondary users is characterized by the interference channel gain ($\Omega_{c_{SR}}, \Omega_{c_{SD}}, \Omega_{c_{RD_1}}, \Omega_{c_{RD_2}}$) and the SNR values. The simulation takes into account these parameters to assess the system performance under varying conditions. Specifically, the power allocation coefficients affect the overall system throughput and outage probability, which are influenced by the channel gain values and the level of interference. By varying these parameters, the simulation explores how changes in power allocation and channel conditions impact the outage performance and system throughput, providing insights into the optimal allocation strategies for different scenarios.

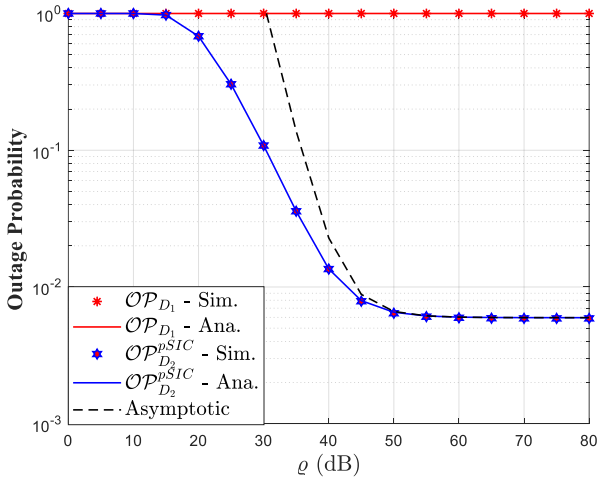

Figure 2. OP versus SNR at D1 and D2.

Figure 2 illustrates the OP versus SNR for both D_1 and D_2, while **Figure 3** shows the system throughput versus SNR. From **Figure 2**, it is evident from the figure that the OP at D_1 (as indicated by the curve) significantly impacts the system throughput of D_1, $\tau_{D_i} = (1 - OP_{D_i})R_1 = (1 - 1)R_1 = 0$, as shown in **Figure 3**. This suggests that for the system throughput to be positive, the minimum power allocation factor (α) must exceed 0.75. This threshold ensures that the allocated power is sufficient to achieve the desired system performance. Conversely, the OP at D_2 and the asymptotic OP exhibit a decreasing trend with increasing SNR, ultimately reaching a point of saturation when the SNR falls between 60 dB and 80 dB. This saturation behavior indicates that beyond a certain SNR level, further increases in SNR do not substantially enhance the OP. These observations can be further explained by the

analytical expressions provided in Equations (14), (18), (19), (23), (24), and (25), which model the relationship between OP, SNR, and power allocation. The equations offer insights into how varying the power allocation impacts the outage performance and system throughput, particularly under high SNR conditions.

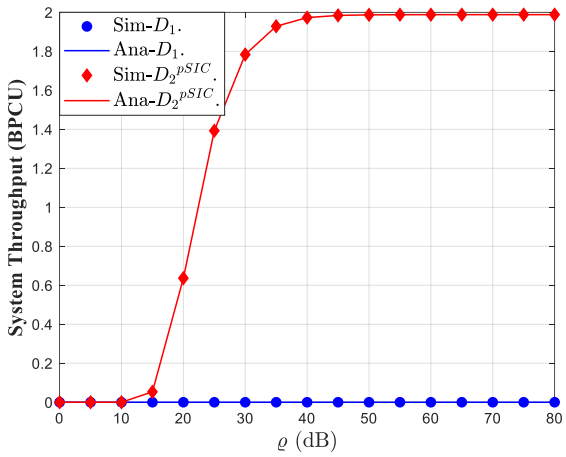

Figure 3. System throughput versus SNR.

Case 2: The simulation parameters were set with specific power allocation coefficients $\alpha_1 = 0.8, \alpha_2 = 0.2$, target rates $R_1 = 1bps/Hz, R_2 = 2bps/Hz$, and channel gain values ($\Omega_{C_{SR}} = 1$, $\Omega_{C_{SD}} = 1$, $\Omega_{C_{RD_1}} = 0.8$, $\Omega_{C_{RD_2}} = 1$), interference between the primary network and SNR,$\varrho_I = 40dB$.

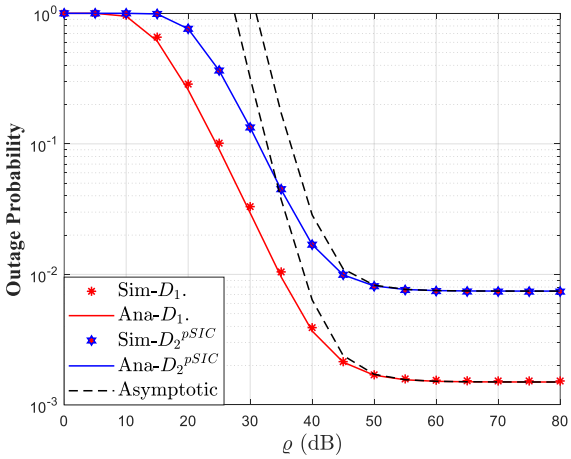

Figure 4. OP versus SNR at D1 and D2.

Figure 4 illustrates that the OP versus SNR at both D_1 and D_2 decreases rapidly as the SNR of the transmission power increases. This trend indicates that with higher SNR values, the likelihood of outage significantly reduces, reflecting improved system performance. The OP at both D_1 and D_2 tends to stabilize within the SNR range of 60 dB to 80 dB, suggesting that beyond this SNR range, further increases in SNR have a diminishing effect on reducing the OP. This stabilization can be attributed to the fact that at high SNR values, the system approaches its optimal performance limits, and additional improvements in SNR contribute less to reducing the OP. These observations are consistent with the theoretical predictions provided in Equations (14),

(18), (19), (23), (24) and (25). These equations capture the relationship between SNR and OP, explaining why the OP decreases rapidly with increasing SNR initially and then levels off as the SNR reaches a certain threshold. The mathematical formulations provide a comprehensive understanding of the system's behavior under varying SNR conditions and offer insights into the performance limits and efficiency of the power allocation strategies.

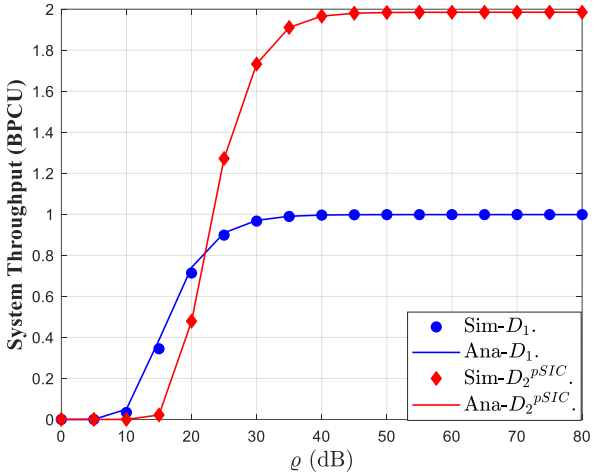

Figure 5. System throughput versus SNR.

Figure 5 illustrates the system throughput versus SNR. Observing **Figure 5**, it can be seen that the system throughput at D_2 is lower than that at D_1 in the low SNR region. However, in the high SNR region, the system throughput at D_2 increases rapidly and is nearly double that of D_1 in the SNR range from 50 dB to 80 dB. This can be explained by the fact that as SNR increases, according to Equation (23), the OP at D_2 decreases more rapidly compared to the OP at D_1 according to Equation (18) in the SNR range from 50 dB to 80 dB. As the OP decreases, according to Equation (26), the system throughput increases

Case 3: The simulation parameters were set with specific power allocation coefficients $\alpha_1 = 0.8$, $\alpha_2 = 0.2$, target rates $R_1 = 1bps/Hz$, $R_2 = 2bps/Hz$, and channel gain values ($\Omega_{c_{SR}} = 1$, $\Omega_{c_{SD}} = 1$, $\Omega_{c_{RD_1}} = 0.8$, $\Omega_{c_{RD_2}} = 1$), interference between the primary network and SNR, $\varrho_I = 40dB$and $\varrho_I = 60dB$.

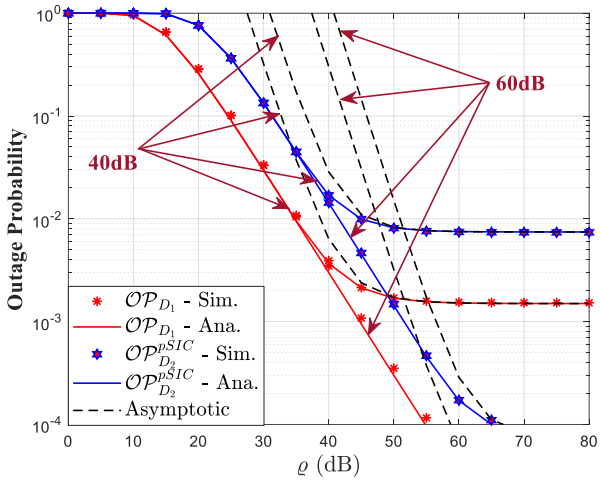

Figure 6. OP versus SNR at D1 and D2 with ϱ I =40dB and ϱ I =60dB.

Figure 6 illustrates the OP at D_1 and D_2 for varying values of $\varrho_I = 40\text{dB}$ ($\varrho_I = 40\text{dB}$ and $\varrho_I = 60\text{dB}$). From **Figure 6**, it is evident that increasing $\tilde{n}_I$ contributes to a reduction in the OP at both D_1 and D_2. This suggests that a higher power allocation to the users leads to improved performance in terms of reduced OP.

However, the system's performance stabilizes at high SNR levels, specifically within the range of 60 dB to 80 dB. Beyond this range, further increases in SNR do not significantly affect the OP. Additionally, there is a noticeable discrepancy between the analytical and simulated OP values at these high SNR levels. This discrepancy could be due to several factors such as imperfections in the theoretical models, approximations made during analytical derivations, or variations in practical implementation details compared to the simulation environment. Understanding and addressing these differences is crucial for improving the accuracy of analytical predictions and ensuring reliable system performance assessments.

Case 4: Increase the power allocation coefficients ($a_I = 0.82$) for D_1 and vary the channel gain values ($\Omega_{c_{SR}} = 1.1, \Omega_{c_{SD}} = 1.1, \Omega_{c_{RD_1}} = 0.8, \Omega_{c_{RD_2}} = 1.1, \varrho_I = 40\text{dB}$).

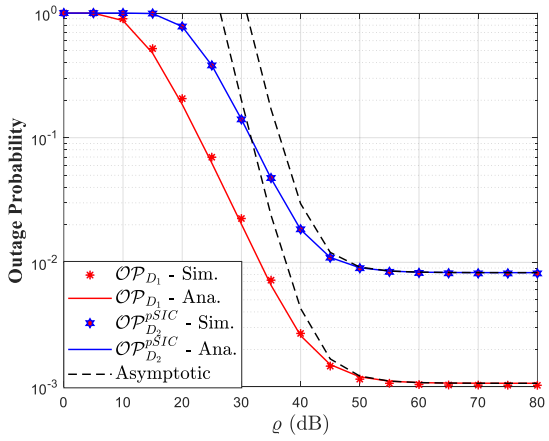

Figure 7. OP at D_1 and D_2 when varying $a_1 = 0.82$, $a_2 = 0.18$,$\Omega_{c_{SR}} = 1.1$,$\Omega_{c_{SD}} = 1.1$,$\Omega_{c_{RD_1}} = 0.8$,$\Omega_{c_{RD_2}} = 1.1$,$\varrho_I = 40dB$.

From **Figure 7**, we observe that the outage probability (OP) at both D_1 and D_2 decreases, indicating improved performance as the system parameters are optimized. Specifically, increasing the interference power (ρ_I) as illustrated in **Figure 6**, or varying the power allocation coefficients and channel gain values as depicted in **Figure 7**, can further reduce the OP to a lower level. This suggests that strategic adjustments, such as increasing ρ_I or optimizing power allocation and channel gain values, can enhance the performance at the destinations within the NOMA system. The results imply that placing relay stations at optimal locations could significantly improve system performance by reducing the OP at both destinations. This placement helps in better managing the power and interference, thus enhancing the overall efficiency of the NOMA system. Additionally, when comparing the OP with respect to the SNR at the secondary source, we find that the OP decreases rapidly in the low SNR region and tends to stabilize in the high SNR region, specifically between 60 dB and 80 dB. This stabilization at high SNR levels indicates that beyond a certain SNR threshold, additional increases do not substantially impact the OP, highlighting the diminishing returns of improving SNR at higher levels.

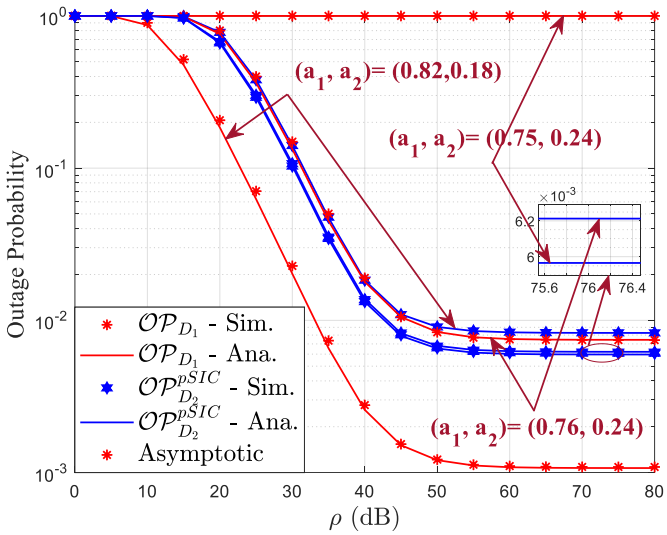

Figure 8. OP versus Signal-to-Noise Ratio (SNR) at D1 and D2 for different pairs of (a1, a2) values.

From **Figure 8**, we observe that as the value of a_1 decreases, the OP at D_1 increases, becoming completely discontinuous when $a_1 = 0.75$. In contrast, the OP at D_2 gradually decreases. This indicates that selecting the appropriate pair of values (a_1, a_2) is crucial for enhancing the overall system performance.

5. Conclusion

In this paper, we have studied the CR-NOMA network over Rayleigh fading channels by establishing explicit and approximate OP expressions for user devices D_1 and D_2. Through rigorous analysis and derivation, we provide clear mathematical expressions that characterize the outage performance for each device under various conditions. Simulations compare the performance of the two user devices in the CR-

NOMA network, offering insights into how different parameters affect their reliability and efficiency. Fairness between the two user devices is satisfied, as demonstrated in the numerical simulation results, by appropriately selecting power allocation factors and SNR. This ensures that both users achieve a balanced quality of service, which is critical for the practical deployment of CR-NOMA systems. Another important consideration is the ability to limit interference to the primary network. We address this by optimizing the secondary users' transmission power while adhering to interference constraints. Furthermore, the comparison results of the OP indicate that D_1 performs better than D_2 in the considered scenarios, highlighting the influence of channel conditions and power allocation on the performance of each device. These findings underscore the importance of strategic resource management in enhancing the robustness and fairness of CR-NOMA networks.

Acknowledgments: The author sincerely thanks the support in terms of time and facilities from Industrial University of Ho Chi minh City for this research.

Conflict of interest: The author declares no conflict of interest.

References

1. Weinberg S. Gravitation and Cosmology. New York: Wiley; 1972.
2. Gu YQ. Dynamical Reason for a Cyclic Universe. Symmetry. 2021; 13(12): 2272. doi: 10.3390/sym13122272
3. Caldwell RR, Dave R, Steinhardt PJ. Cosmological Imprint of an Energy Component with General Equation of State. Physical Review Letters. 1998; 80(8): 1582–1585. doi: 10.1103/physrevlett.80.1582
4. Turner MS. Dark Matter and Dark Energy in the Universe. Physica Scripta. 2000; T85(1): 210. doi: 10.1238/physica.topical.085a00210
5. Peebles PJE, Ratra B. The cosmological constant and dark energy. Reviews of Modern Physics. 2003; 75(2): 559–606. doi: 10.1103/revmodphys.75.559
6. Carroll SM. Quintessence and the Rest of the World: Suppressing Long-Range Interactions. Physical Review Letters. 1998; 81: 3067. doi: 10.1103/PhysRevLett.81.3067
7. Zlatev I, Wang LM, Steinhardt PJ. Quintessence, Cosmic Coincidence, and the Cosmological Constant. Physical Review Letters. 1999; 82: 896-899. doi: 10.1103/PhysRevLett.82.896
8. Faraoni V. Inflation and quintessence with nonminimal coupling. Physical Review D. 2000; 62: 023504. doi:10.1103/PhysRevD.62.023504
9. Gasperini M, Piazza F, Veneziano G. Quintessence as a runaway dilaton. Physical Review D. 2002; 65: 023508. doi: 10.1103/PhysRevD.65.023508
10. Capozziello S. Curvature Quintessence. International Journal of Modern Physics D. 2002; 11: 483. doi: 10.1142/S0218271802002025
11. Caldwell RR, Linder EV. Limits of Quintessence. Physical Review letter. 2005; 95: 141301. doi: 10.1103/PhysRevLett.95.141301
12. Astashenok AV, Nojiri S, Odintsov SD, Scherrer RJ. Scalar dark energy models mimicking ΛCDM with arbitrary future evolution. Physics Letters B. 2012; 713: 145-153. doi: 10.1016/j.physletb.2012.06.017
13. Tsujikawa S. Quintessence: A review. Quantum Gravity. 2013; 30: 214003. doi: 10.1088/0264-9381/30/21/214003
14. Shahalam M, Pathak SD, Verma MM, et al. Dynamics of interacting quintessence. The European Physical Journal C. 2015; 75(8): 395. doi: 10.1140/epjc/s10052-015-3608-1
15. Han C, Pi S, Sasaki M. Quintessence saves Higgs instability. Physics Letters B. 2019; 791: 314-318. doi: 10.1016/j.physletb.2019.02.037
16. Sahni V. The cosmological constant problem and quintessence. Classical and Quantum Gravity. 2002; 19(13): 3435–3448. doi: 10.1088/0264-9381/19/13/304

17. S. Turner M, Huterer D. Cosmic Acceleration, Dark Energy, and Fundamental Physics. Journal of the Physical Society of Japan. 2007; 76(11): 111015. doi: 10.1143/jpsj.76.111015
18. Ishak M. Remarks on the Formulation of the Cosmological Constant/Dark Energy Problems. Foundations of Physics. 2007; 37(10): 1470–1498. doi: 10.1007/s10701-007-9175-z
19. Szydłowski M, Kurek A, Krawiec A. Top ten accelerating cosmological models. Physics Letters B. 2006; 642(3): 171–178. doi: 10.1016/j.physletb.2006.09.052